Experimental and Computational Studies of Nucleophilic Attack, Tautomerization, and Hydride Migration in Benzoheterocycle Triosmium Clusters

Djamaladdin G. Musaev,* Taraneh Nowroozi-Isfahani, and Keiji Morokuma*

Emerson Center for Scientific Computation and Department of Chemistry, 1515 Dickey Drive, Emory University, Atlanta, Georgia 30322

Joynal Abedin and Edward Rosenberg*

Department of Chemistry, University of Montana, Missoula, Montana 59812

Kenneth I. Hardcastle

Department of Chemistry, 1515 Dickey Drive, Emory University, Atlanta, Georgia 30322

Received August 19, 2005

The reactions of $Os_3(CO)_9(\mu_3\text{-}\eta^2\text{-(L-H)})(\mu\text{-H})$ (L = benzothiazole (**7**), benzoxazole (**8**)) with H^-/H^+ are reported, We observe only nucleophilic attack at the 2-position followed by protonation at the metal core to yield the 48e μ-amido−aryl complexes $Os_3(CO)_9(\mu_3\text{-}\eta^2\text{-(L-H)})(\mu\text{-H})_2$ (L = benzothiazole (**9**), benzoxazole (**10**)). The solid-state structure of **9** is reported. On thermolysis these complexes tautomerize to the corresponding μ-alkylidene−imino complexes **11** (L = benzothiazole) and **12** (L = benzoxazole) with equilibrium constants of **11/9** = 1.6 and **12/10** = 3.1. The tautomerization takes place with first-order rate constants of $(6.42 \pm 0.6) \times 10^{-5}$ and $(1.28 \pm 0.1) \times 10^{-4}$ s^{-1} for **9** → **11** and **10** → **12**, respectively. Substitution of a methyl group at the 2-position in the case of **7** changes the site of hydride attack to the 4-position and results in the formation of the $\sigma-\pi$-vinyl complex $Os_3(CO)_9(\mu_3\text{-}\eta^3\text{-(2-CH}_3)C_7H_5NS)(\mu\text{-H})$ (**9′**). The complexes $Os_3(CO)_9(\mu_3\text{-}\eta^2\text{-(L-2H)})(\mu\text{-H})_2$ (L = tetrahydroquinoline (**3**), indoline (**4**)) also tautomerize to the corresponding μ-amido−aryl complexes $Os_3(CO)_9(\mu_3\text{-}\eta^2\text{-(L-2H)})(\mu\text{-H})_2$ (L = tetrahydroquinoline (**5**), indoline (**6**)) at approximately the same rates as **9** and **10** and have similar equilibrium constants. Density functional theory (DFT) calculations reveal that the tautomerization in these systems proceeds via a four-center transition state. The calculated barriers for tautomerization are in reasonable agreement with the experimental data. DFT calculations on **6** reveal that the lower energy transition state for hydride migration is an unsymmetrically face-bridged hydride rather than a terminal hydride. Natural population analysis (NPA) of the optimized structures of the 46e clusters and their corresponding free ligands reveals that the site of nucleophilic attack can be predicted on the basis of the net charge on the C−H groups on the heterocyclic rings and/or the relative stability of the resulting anions.

Introduction

The impact of the bonding mode of an organic ligand on the regiochemistry of nucleophilic attack is a subject of great interest to organic and organometallic chemists.[1] In the particular case of polymetallic complexes, there appears to be a delicate balance between steric and electronic effects that determines whether the site of nucleophilic attack is on the metal core, on an ancillary ligand such as CO, or on one or more of several possible positions on the coordinated organic ligands.[2] This is especially true of the trimetallic clusters of ruthenium and osmium, where the stability of the metal frameworks has led to a very rich organometallic chemistry.[3]

Over the past several years we have been studying the chemistry of benzoheterocyclic complexes of triosmium clusters. The impact on the site of nucleophilic attack of the bonding mode of the heterocyclic ligand to the metal core and the nature of the incoming nucleophile is particularly dramatic in this series of complexes. Thus, in the case of the 46e quinoline complex $Os_3(CO)_9(\mu_3\text{-}\eta^2\text{-(L-H)})(\mu\text{-H})$ (L = quinoline (**1**)),

(1) Tsuji, J. *Transition Metal Reagents and Catalysis*; Wiley: Chichester, U.K., 2000.

(2) Lavigne, G. In *The Chemistry of Metal Cluster Complexes*; Shriver, D. F., Kaesz, H. D., Adams, R. D., Eds.; VCH: New York, 1990; Chapter 5.

(3) For recent comprehensive reviews on ruthenium and osmium carbonyl cluster chemistry, see: (a) Deeming, A. J. In *Comprehensive Organometallic Chemistry II*; Abel, E. W., Stone, F. G. A., Wilkinson, G., Eds.; Pergamon: Oxford, U.K., 1995; Vol. 7, p 684. (b) Smith, A. K. In *Comprehensive Organometallic Chemistry II*; Abel, E. W., Stone, F. G. A., Wilkinson, G., Eds.; Pergamon: Oxford, U.K., 1995; Vol. 7, p 747. (c) Sappa, E. In *Comprehensive Organometallic Chemistry II*; Abel, E. W., Stone, F. G. A., Wilkinson, G., Eds.; Pergamon: Oxford, U.K., 1995; Vol. 7, p 804. (d) Pomeroy, R. K. In *Comprehensive Organometallic Chemistry II*; Abel, E. W., Stone, F. G. A., Wilkinson, G., Eds.; Pergamon: Oxford, U.K., 1995; Vol. 7, p 836. (e) Cifuentes, M. P.; Humphrey, M. G. In *Comprehensive Organometallic Chemistry II*; Abel, E. W., Stone, F. G. A., Wilkinson, G., Eds.; Pergamon: Oxford, U.K., 1995; Vol. 7, p 908.

10.1021/om050719l CCC: $33.50
Publication on Web 12/02/2005

nucleophilic attack occurs at the 5-position with carbanions and hydride to give the $\sigma-\pi$-vinyl complexes after protonation but at the metal core with neutral nucleophiles such as phosphine and amine (eq 1).[4,5] In the case of the 3,4-

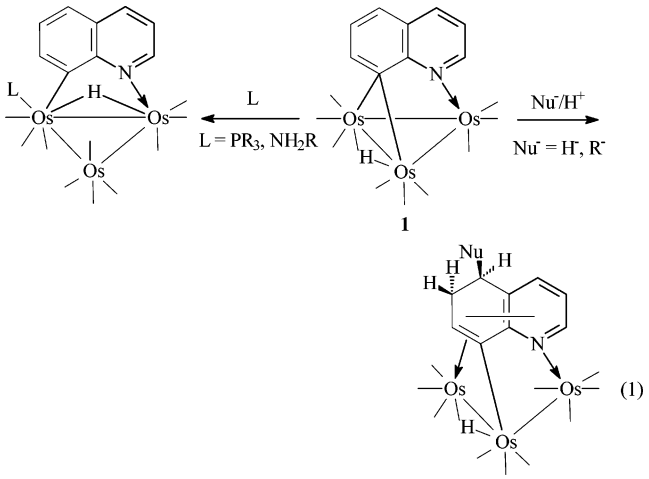

dihydroquinoline complex $Os_3(CO)_9(\mu_3\text{-}\eta^2\text{-(L-H)})(\mu\text{-H})$ (L = 3,4-dihydroquinoline (**2**)) nucleophilic attack reverts to the 2-position of the heterocyclic ring, which is the normal site of nucleophilic attack in the free ligand, to give the μ-alkylidene−imino complex $Os_3(CO)_9(\mu_3\text{-}\eta^2\text{-(L-2H)})(\mu\text{-H})_2$ (L = tetrahydroquinoline (**3**)) following protonation at the metal core (eq 2).[5] Complex **3** and its indoline analogue, $Os_3(CO)_9(\mu_3\text{-}\eta^2\text{-}$

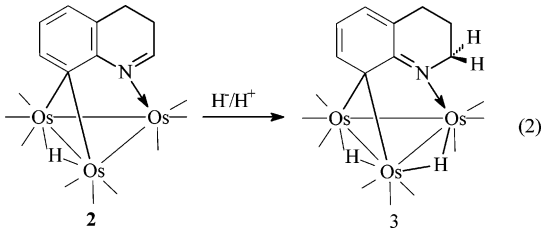

$(L\text{-}2H))(\mu\text{-H})_2$ (L-2H = indoline (**4**)), are also obtained by the reaction of 1,2,3,4-tetrahydroquinoline or indoline with $Os_3(CO)_{10}(CH_3CN)_2$ at 25−60 °C, respectively.[6] Most interestingly, at 90 °C complexes **3** and **4**, containing the bridging alkylidene, slowly tautomerize to the slightly thermodynamically more stable μ-amido−aryl isomers **5** and **6**, respectively (eqs 3 and 4).

The tautomeric pairs **3**/**5** and **4**/**6** represent very unusual tautomeric equilibria where the magnitude of the equilibrium constants is small but the rate of tautomerization is slow ($(2.4 \pm 0.2) \times 10^{-5}$ and $(6.4 \pm 0.6) \times 10^{-5}$ for **3** and **4**, respectively).[6] The nature of the transition states involved in the tautomerizations of **3** to **5** and **4** to **6** is not known.

In a related study we reported that for complexes of structural type **1** with benzothiazole, $Os_3(CO)_9(\mu_3\text{-}\eta^2\text{-(L-H)})(\mu\text{-H})$ (L = benzothiazole (**7**)), on reaction with the relatively bulky carbanion lithium isobutyronitrile, nucleophilic attack in **7** occurs at the 4-position whether the substituent at the 2-position is

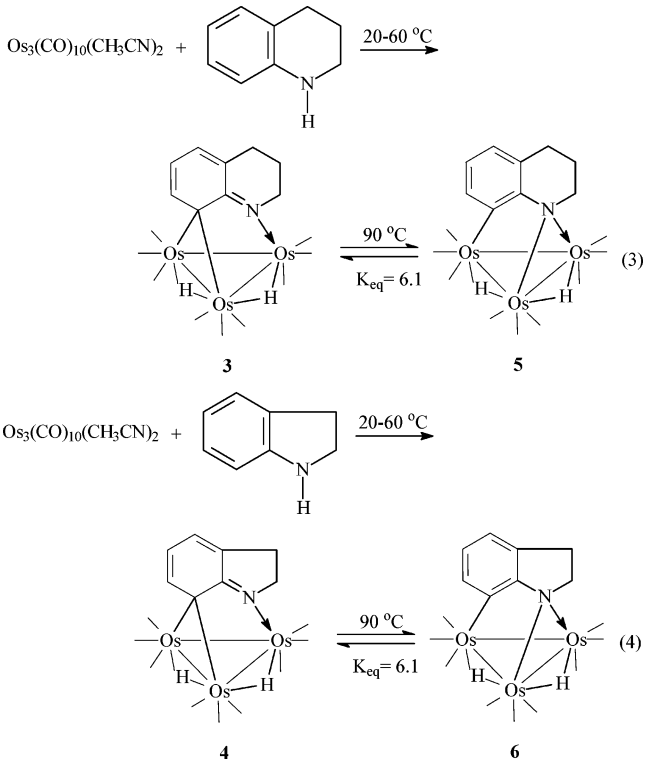

H or CH_3 (eq 5), while the 2-position is where nucleophilic

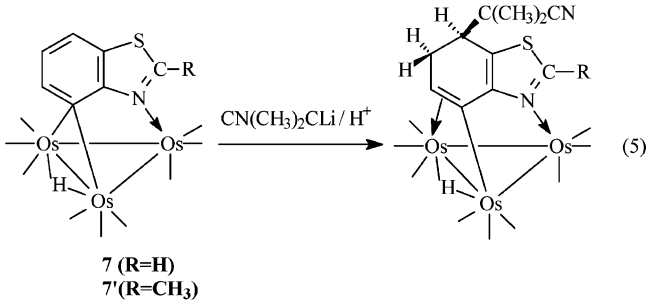

attack takes place in the free ligand.[7] We report here that reaction of **7** and the analogous benzoxazole complex $Os_3(CO)_9(\mu_3\text{-}\eta^2\text{-(L-H)})(\mu\text{-H})$ (L = benzoxazole (**8**)) with H^- results in nucleophilic attack at the 2-position when R = H for **7** and **8** and at the 4-position when R = CH_3 for **7′**. Protonation of the resulting anions $\mathbf{7H}^-$ and $\mathbf{8H}^-$ takes place at the metal core for both species but gives the μ-amido−aryl structure as the kinetic product, which slowly tautomerizes to the μ-alkylidene−imino structure at elevated temperatures, exactly the opposite of what was observed for the heterocyclic complexes of 1,2,3,4-tetrahydroquinoline and indoline **3** and **4** (eqs 3 and 4). The reasons for this apparent reversal in the nature of the kinetic product formed could relate to the structure of the intermediate anions or to the kinetic site of protonation of a common intermediate.

In light of the recent successes in using quantum-mechanical methods, in particular the density functional theory (DFT) method, for understanding the energetics and reaction dynamics of organometallic complexes, we have undertaken a computational study on the complexes referred to above.[8−18] The goals

(4) Bergman, B.; Holmquist, R. H.; Smith, R.; Rosenberg, E.; Hardcastle, K. I.; Visi, M.; Ciurash, J. *J. Am. Chem. Soc.* **1998**, *120*, 12818.

(5) Rosenberg, E.; Arcia, E.; Kolwaite, D. S.; Hardcastle, K. I.; Ciurash, J.; Duque, R.; Gobetto, R.; Milone, L.; Osella, D.; Botta, M.; Dastrú, W.; Viale, A.; Fiedler, J. *Organometallics* **1998**, *17*, 415.

(6) Rosenberg, E.; Kolwaite, D. S.; Kabir,. S. E.; Hardcastle, K. I.; McPhillips, T.; Duque, R.; Day, M. *Organometallics* **1996**, *15*, 1979.

(7) Rosenberg, E.; Abedin, J.; Kabir, S. E.; Hardcastle, K. I. *Organometallics* **2004**, *23*, 3982.

(8) Kim, K. H.; Jung, J.; Han, Y. K. *Organometallics* **2004**, *23*, 3865.

(9) Bergamo, M.; Beringhelli, T.; D'Alphoso, G.; Garavaglia, L.; Mercandelli, P.; Moret, M.; Sironi, A. *J. Cluster Sci.* **2001**, *12*, 223.

(10) Khoroshun, D. V.; Inagaki, A.; Suzuki, H.; Vyboishchikov, S. F.; Musaev, D. G.; Morokuma, K. *J. Am. Chem. Soc.* **2003**, *125*, 9910.

of these studies are (1) to identify the nature of the transition states for the observed tautomerizations and (2) to understand the factors contributing to the regioselective nature of nucleophilic attack on these species. The results of these studies are reported here, along with the experimental details of the reactions of **7** and **8** with H^-/H^+ and the kinetics of tautomerization of the products of these reactions.

Experimental Section

General Considerations. All reactions were performed under a dry nitrogen or argon atmosphere in a two-necked flask using standard Schlenk techniques or in an M-Braun (manual MB-150-M) drybox. The flask was flame-dried under vacuum for every reaction. Dichloromethane was distilled from CaH_2, and trifluoroacetic acid (Aldrich) was distilled from phosphorus pentoxide prior to use. Lithium triethylborohydride and dichloromethane-d_2 were purchased from Aldrich Chemical Co., and the latter was dried over freshly activated molecular sieves (type 4a, Mallinckrodt). Complexes **7** and **8** were synthesized according to published literature procedures.[19] Thin-layer chromatography was performed on 20 × 40 cm glass plates using a 2 mm layer of silica gel PF-254 (E & M Science). Two or three elutions were necessary to obtain adequate resolution of the bands. Infrared data were obtained on a Thermo-Nicolet 633 FT IR spectrometer, and NMR spectra were obtained on a Varian 400 MHz Unity Plus NMR. Schwarzkopf Microanalytical Laboratories, Woodside, NY, performed elemental analyses.

Reactions of $Os_3(CO)_9(\mu_3\text{-}\eta^2\text{-}C_7H_3(2\text{-}R)NX)(\mu\text{-}H)$ (R = H, X = S, 7; R = CH_3, X = S, 7′; R = H, X = O, 8) with $LiEt_3BH$ and CF_3COOH. Dark green crystals of **7** (100 mg, 0.10 mmol), **7′** (100 mg, 0.10 mmol), or **8** (100 mg, 0.10 mmol) were dissolved in 25 mL of CH_2Cl_2 in a 50 mL two-necked round-bottom flask that was fitted with a gas inlet tube and evacuated and filled with argon. A 1.0 M solution of $LiEt_3BH$ (105 μL, 0.10 mmol) in THF was then added dropwise to the cluster solution, and a color change was observed from green to orange for all of these clusters. The solution was then neutralized with CF_3COOH (~8.1 μL, 0.10 mmol). A color change was observed from orange to yellow. The solvent was removed under vacuum. The residue was taken up in dichloromethane and chromatographed by TLC on silica gel. Elution with hexane/CH_2Cl_2 (3:1) gave the complex **9** (80 mg) for **7**, **9′** (75 mg) for **7′**, and **10** for **8** (42 mg) in 79, 74, and 41% yields, respectively, after recrystallization from dichloromethane/hexane.

Analytical and Spectroscopic Data for 9. Anal. Calcd for $C_{16}H_7NSO_9Os_3$: C, 20.02; H, 0.73; N, 1.46. Found: C, 19.99; H, 0.49; N, 1.03. IR (ν(CO)) in CH_2Cl_2: 2083 s, 2051 s, 2026 w, 2008 w, br, 1994 w, br, cm^{-1}. ^1H NMR in $CDCl_3$ (at 22 °C): δ 7.21 (dd, H(6)), 6.62 (dd, H(4)), 6.56 (d of t, H(5)), 5.2−3.9 (br, 2H(2)), −14.06 (s, hydride). ^1H NMR of **9** in $CDCl_3$ (at −45 °C): δ 7.21 (dd, H(6)), 6.62 (dd, H(4)), 6.56 (d of t, H(5)), 5.05 (d, J = 12 Hz, H(2)), 3.95 (d, J = 12 Hz, H(2)), −14.06 (s, J = 2 Hz, hydride), −14.10 (s, J = 2 Hz, hydride).

Analytical and Spectroscopic Data for 9′. Anal. Calcd for $C_{17}H_9NSO_9Os_3$: C, 20.97; H, 0.92; N, 1.41. Found: C, 21.13; H, 0.70; N, 1.10. IR (ν(CO)) in CH_2Cl_2: 2077 m, 2047 s, 2021 s, 1989 s, br, 1971 w, br cm^{-1}. ^1H NMR in $CDCl_3$: δ 4.46 (dd, H(6)), 2.65 (m, 2H(4)), 2.38 (m, H(5)), 2.62(s, $-CH_3$), −16.93 (s, hydride).

Spectroscopic Data for 10. IR (ν(CO)) in CH_2Cl_2: 2078 m, 2051 s, 2024 w, br 1992 w, br, 1967 w, br cm^{-1}. ^1H NMR in $CDCl_3$ (22 °C): δ 6.96 (d, H(6)), 6.28 (d, H(4)), 6.53 (t, H(5)), 5.17 (br, 2H(2)), −13.95 (s, hydride). ^1H NMR in $CDCl_3$ (at −45 °C): δ 6.96 (d, H(6)), 6.28 (d, H(4)), 6.53 (t, H(5)), 5.04 (d, J = 5 Hz, H(2)), 5.28 (d, J = 5 Hz, H(2)), −13.84 (s, hydride), −14.07 (s, hydride).

Evaluation of Equilibrium Constants (K_{eq}) and Rate Constant Measurements for the Tautomerization of 9 to 11 and 10 to 12. Solutions of **9** and **10** (30 mg, ~0.03 mmol) in 0.6 mL of $C_6D_5CD_3$ in two separate 5 mm sealed NMR tubes were heated to 90 °C and their ^1H NMR spectra were checked every 2 h at ambient temperature. When there was no further change in the hydride region, K_{eq} was calculated from the integration of the hydride peaks of **9** and **11** and **10** and **12**, respectively.

Solutions of **9** and **10** (0.02 mmol) in 0.6 mL of CD_6CD_3 in sealed 5 mm NMR tubes were heated to 90 °C in the NMR probe, and a ^1H NMR spectrum was taken every 1 h for **9** and every $^1/_2$ h for **10** for 15 h. The rate constants for the conversions of **9** to **11** and **10** to **12** were evaluated by measuring the relative intensities of each isomer and plotting the values ln C versus t using the equation $\ln C = \ln C_0 - kt$. The errors reported are ±10% on the basis of the expected error in relative integrated intensities for the NMR technique (±5%).

Spectroscopic Data for 11. IR (ν(CO)) in CH_2Cl_2: 2082 s, 2050 s, 2023 w, 2005 w, br, 1993 w, br 1976 w, br cm^{-1}. ^1H NMR of **11** in $CDCl_3$: δ 6.88 (dd, H(6)), 6.34 (dd, H(4)), 5.45 (d of t, H(5)), 5.02 (d, J = 12 Hz, H(2)), 4.79 (d, J = 12 Hz, H(2)), −13.05 (d J = 2 Hz, hydride), −13.43 (d, J = 2 Hz, hydride).

Spectroscopic Data for 12. IR (ν(CO)) in CH_2Cl_2: 2076 m, 2051 s, 2022 w, br, 1990 w, br, 1966 w, br cm^{-1}. ^1H NMR of **12** in $CDCl_3$: δ 6.25 (d, H(6)), 6.14 (d, H(4)), 5.50 (t, H(5)), 5.47 (d, J = 8 Hz, H(2)), 5.30 (d, J = 5 Hz, H(2)), −13.16 (d, J = 2 Hz, hydride), −13.22 (d, J = 2 Hz, hydride) ppm.

Computational Procedures. Geometries and energetics of the proposed structures and transition states of the numerous intramolecular transformations of these species were calculated using the B3LYP density functional method[20] in conjunction with the standard LANL2DZ basis set of Hay and Wadt for Os atoms and 6-31(d) basis sets for the other elements.[21] The nature of all stationary points was confirmed by performing a normal-mode analysis. In addition, the nature of the calculated transition states was clarified using the pseudo-intrinsic reaction coordinates (IRC) approach.[22,23] The enthalpy (H) and Gibbs free energy (G) calculations of the systems were performed at 298.15 K and 1 atm of pressure. All calculations were performed without symmetry constraints utilizing the Gaussian03 program.[24] Where appropriate, the chemically more interesting ΔH values will be used in the discussion and corresponding ΔG values will be given in parentheses. Note that the difference between ΔG and ΔH surfaces reflects the entropy contribution. In comparisons with experimentally measured equilibrium constants or rate constants estimated at a single temperature with calculated values, ΔG or $\Delta G^{\ddagger}$ will be used.

(11) Riehl, J. F.; Koga, K.; Morokuma, K. *J. Am. Chem. Soc.* **1994**, *116*, 5414.
(12) Riehl, J. F.; Koga, K.; Morokuma, K. *J Organometallics* **1994**, *13*, 4765.
(13) Riehl, J. F.; Koga, K.; Morokuma, K. *J Organometallics* **1993**, *12*, 4788.
(14) Zimmerman, C.; Anson, C. E.; Eckerman, A. L.; Wunder, M.; Fischer, G.; Keihauer, I.; Herrling, E.; Pilawa, B.; Hampe, O.; Weigand, F.; Dehnen, S. *Inorg. Chem.* **2004**, *43*, 4595.
(15) Wadepohl, H.; Castano, M. E. *Chem. Eur. J.* **2003**, *9*, 5266.
(16) Morioka, T.; Ozawa, S.; Yamabe, T.; Masuda, H. *Polyhedron* **2003**, *22*, 3413.
(17) Wong, W. Y.; Choi, K. H.; Lin, Z. *Eur. J. Inorg. Chem.* **2002**, 2112.
(18) Kaupp, M. *Chem. Commun.* **1996**, 1141.
(19) Abedin, J.; Bergman, B.; Holmquist, R.; Smith, R.; Rosenberg, E.; Ciurash, J.; Hardcastle, K. I.; Roe, J.; Vazquez, V.; Roe, C.; Kabir, S. E.; Roy, B.; Alam, S.; Azam, K. A. *Coord. Chem. Rev.* **1999**, *190−192*, 975.
(20) (a) Becke, A.D. *Phys. Rev. A* **1988**, *38*, 3098. (b) Lee, C.; Yang, W.; Parr, R. G. *Phys. Rev. B* **1988**, *37*, 785. (c) Becke, A. D. *J. Chem. Phys.* **1993**, *98*, 5648.
(21) (a) Hay, P. J.; Wadt, W. R. *J. Chem. Phys.* **1985**, *82*, 270. (b) Hay, P. J.; Wadt, W. R. *J. Chem. Phys.* **1985**, *82*, 284. (c) Hay, P. J.; Wadt, W. R. *J. Chem. Phys.* **1985**, *82*, 299.
(22) Fukui, K. *Acc. Chem. Res.* **1981**, *14*, 363.
(23) We have performed 10 steps of IRC (forward and reverse) calculations followed by the optimization of geometries.
(24) Frisch, M. J., et al. *Gaussian 03*, Revision C.02; Gaussian, Inc., Wallingford, CT, 2004.

Table 1. Crystal Data and Structure Refinement Details for 9

empirical formula	$C_{16}H_7NO_9Os_3S$
formula wt	959.89
temp	100(2) K
wavelength	0.710 73 Å
cryst syst	monoclinic
space group	$P2_1$
unit cell dimens	$a = 8.8775(8)$ Å
	$b = 15.4784(15)$ Å
	$c = 14.9072(14)$ Å
	$\alpha = 90$
	$\beta = 91.650(2)$
	$\gamma = 90$
V	2047.5(3) Å^3
Z	4
density (calcd)	3.114 Mg/m^3
abs coeff	18.721 mm^{-1}
$F(000)$	1704
cryst size	0.08 × 0.04 × 0.01 mm^3
θ range for data collecn	1.90−33.13°
index ranges	$-13 \le h \le 13$, $-22 \le k \le 23$, $-22 \le l \le 22$
no. of rflns collected	26 830
no. of indep rflns	13 598 (R(int) = 0.0816)
completeness to $\theta = 33.13°$	93.7%
abs cor	semiempirical from equivalents
max and min transmissn	1.0000 and 0.223086
refinement method	full-matrix least squares on F^2
no. of data/restraints/params	13 598/1/281
goodness of fit on F^2	1.047
final R indices ($I > 2\sigma(I)$)	R1 = 0.0692, wR2 = 0.1320
R indices (all data)	R1 = 0.1088, wR2 = 0.1456
absolute struct param	0.03(2)
largest diff peak and hole	6.087 and −3.052 e Å^{-3}

X-ray Structure Determination of Compound 9. A suitable crystal of **9** was coated with Paratone N oil, suspended in a small fiber loop, and placed in a cooled nitrogen gas stream at 100 K on a Bruker D8 SMART APEX CCD sealed-tube diffractometer with graphite-monochromated Mo Kα (0.710 73 Å) radiation. Data were measured using a series of combinations of ψ and ω scans with 10 s frame exposures and 0.3° frame widths. Data collection, indexing, and initial cell refinements were all carried out using SMART[25] software. Frame integration and final cell refinements were done using SAINT[26] software. The final cell parameters were determined from least-squares refinement on 6877 reflections. The SADABS[27] program was used to carry out absorption corrections.

The structure was solved using direct methods and difference Fourier techniques (SHELXTL, version 5.10).[28] Hydrogen atoms were placed in their expected chemical positions using the HFIX command or were located in a difference Fourier and were included in the final cycles of least squares with isotropic U_{ij}'s related to the atom ridden upon. All non-hydrogen atoms were refined anisotropically. Scattering factors and anomalous dispersion corrections are taken from ref 29. Structure solution, refinement, graphics, and generation of publication materials were performed by using SHELXTL version 5.10 software. Additional details of data collection and structure refinement are given in Table 1.

The crystals of **9** were all thin needles and did not diffract too well. The results presented are from the best crystal available. Also, a number of space groups were evaluated, but the data consistently indicated that $P2_1$ was the appropriate one. This gave two molecules in the asymmetric unit of the cell; the molecules differed only slightly in their configurations. All higher symmetry space groups were unsatisfactory; therefore, it is assumed that $P2_1$ is the proper space group. There are pairwise interactions between the sulfur atom on one cluster and carbonyl oxygen on another and between H13 and a carbonyl oxygen on an adjacent molecule.

Scheme 1

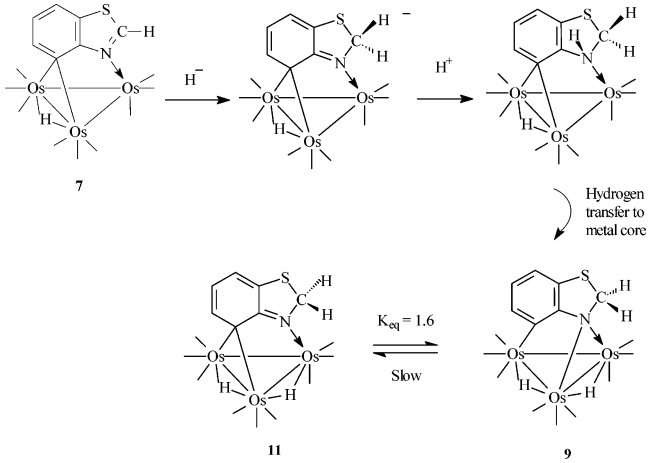

Results and Discussion

Reactions of $Os_3(CO)_9(\mu_3\text{-}\eta^2\text{-}C_7H_3(2\text{-}R)NX)(\mu\text{-}H)$ (R = H, X = S, 7; R = CH_3, X = S, 7′; R = H, X = O, 8) with $LiEt_3BX$ (X = H, D) and CF_3COOH. Reaction of the complex $Os_3(CO)_9(\mu_3\text{-}\eta^2\text{-}C_7H_4NS)(\mu\text{-}H)$ (**7**) with $LiEt_3BH$ results in attack at the C-2 position of the heterocyclic ring, as evidenced by the changes in the ^{1}H NMR spectrum. The resonances for C-4, C-6, and C-5 protons are observed as two doublets at 6.31 and 6.84 ppm and a doublet of doublets at 5.25 ppm, respectively. A proton resonance of relative intensity 2 is observed at 5.06 ppm and is assigned to the newly formed methylene group at the 2-position.

Treatment of this anionic intermediate with CF_3CO_2H was followed by ^{1}H NMR and results in at least partial protonation at the nitrogen atom of the heterocyclic ring, as evidenced by the appearance of a broad resonance at 7.12 ppm and a new hydride resonance at −14.03 ppm in a relative intensity of 1:1 (Scheme 1).

Both of these resonances integrate in a 1:1 relative intensity with three aromatic protons at 7.68 (dd, H(6)), 6.80 (dd, H(4)) and 6.38 ppm (d of t, H(5)) and 1:2 with methylene protons appearing as a doublet at 5.30 ppm. Protonation at the metal core is simultaneously observed, as evidenced by the appearance of a second new hydride singlet at −14.06 ppm integrating in a relative intensity of 2:1 with companion peaks at 6.21 (dd, H(6)), 6.62 (dd, H(4)), and 6.56 ppm (dd, H(5)). A very broad resonance of approximate integrated intensity 2 relative to the aromatic resonances is detected at 5.2−3.9 ppm, suggesting that a hydride exchange process is occurring in the intermediate exchange regime which averages the methylene protons (vide infra). These data are consistent with initial or competitive protonation at nitrogen to give $Os_3(CO)_9(\mu_3\text{-}\eta^2\text{-}C_7H_5N(H)S)(\mu\text{-}H)$, followed by transfer of the proton to the metal core to give $Os_3(CO)_9(\mu_3\text{-}\eta^2\text{-}C_7H_5NS)(\mu\text{-}H_2)$ (**9**; Scheme 1). Upon workup only **9** is isolated in 79% yield. The exact opposite of this process (i.e. initial protonation at the metal core followed by transfer to nitrogen) was observed for **5** and **6**, which are converted to **3** and **4** after deprotonation.[6]

(25) SMART Version 5.624; Bruker AXS, Inc., Analytical X-ray Systems, 5465 East Cheryl Parkway, Madison WI 53711-5373, 2000.
(26) SAINT Version 6.02; Bruker AXS, Inc., Analytical X-ray Systems, 5465 East Cheryl Parkway, Madison WI 53711-5373, 2000.
(27) Sheldrick, G. SADABS Version 2.03; University of Göttingen, Göttingen, Germany, 2001.
(28) SHELXTL Version 5.10; Bruker AXS, Inc., Analytical X-ray Systems, 5465 East Cheryl Parkway, Madison WI 53711-5373, 2000.
(29) *International Tables for X-ray Crystallography*; Wilson, A. J. C.. Ed.; Kynoch Academic: Dordrecht, The Netherlands, 1992; Vol. C, Tables 6.1.1.4 (pp 500−502) and 4.2.6.8 (pp 219−222).

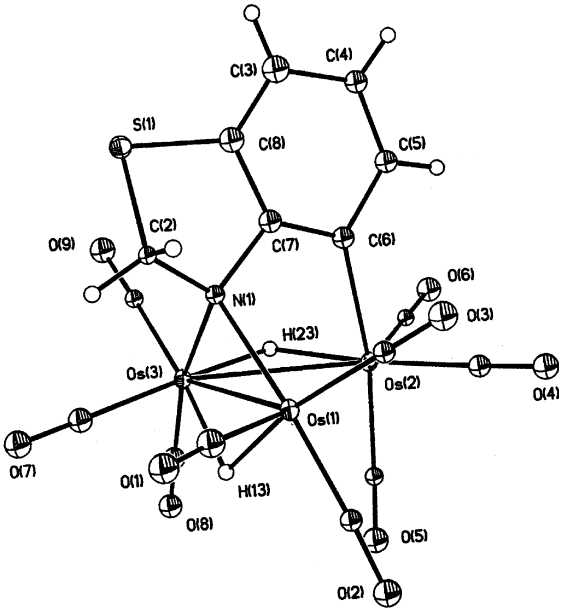

Figure 1. Solid-state structure of $Os_3(CO)_9(\mu_3\text{-}\eta^2\text{-}C_7H_5NS)(\mu\text{-}H_2)$ (**9**).

Table 2. Selected Bond Distances (Å) and Angles (deg) for 9[a]

	Distances		
Os(1)−Os(2)	2.80008(11)	C(7)−C(8)	1.39(3)
Os(1)−Os(3)	2.7909(11)	C(3)−C(4)	1.38(5)
Os(2)−Os(3)	3.0070(11)	C(6)−C(7)	1.39(5)
Os(1)−N(1)	2.162(16)	C(4)−C(5)	1.38(5)
Os(3)−N(1)	2.104(16)	C(5)−C(6)	1.45(3)
C(6)−Os(2)	2.11(2)	C(3)−C(8)	1.36(3)
C(2)−S(1)	1.81(6)	N(1)−C(2)	1.51(2)
C(7)−N(1)	1.47(3)	Os−CO	1.91(2)[b]
C−O	1.12(3)[b]		
	Angles		
Os(2)−Os(1)−Os(3)	65.06(3)	C(6)−C(7)−N(1)	119.7(2)
Os(1)−Os(2)−Os(3)	57.31(3)	C(5)−C(6)−Os(2)	128.5(2)
Os(2)−Os(3)−Os(1)	57.63(3)	Os(3)−N(1)−Os(1)	81.7(5)
Os−C−O	173.1(2)[b]		

[a] Numbers in parentheses are estimated standard deviations. [b] Average values.

On the basis of the ^{1}H NMR data the structure of **9** is analogous to those of **5** and **6**, and before discussing the ligand dynamics of **9**, it is appropriate to confirm its structure in the solid state. The solid-state structure of **9** is shown in Figure 1, crystal data are given in Table 1, and selected distances and bond angles are given in Table 2.

The structure of **9** consists of an isosceles triangle of osmium atoms with two bonds of approximately equal length (Os(1)−Os(2) = 2.80(1) Å and Os(1)−Os(3) = 2.79(1) Å). The elongated edge (Os(2)−Os(3) = 3.00(1) Å) is bridged by the more in-plane hydride ligand, H(23), and the shortest edge is doubly bridged by the single atom amido bridge and a highly tucked hydride ligand, H(13). It is clear from the average C−C distance of 1.39(3) Å that the carbocyclic ring has considerable aromatic character. The N(1)−C(7) and N(1)−C(2) bond lengths (1.47(3) and 1.52(2) Å, respectively) are clearly single bonds. As expected, the C(6)−Os(2) bond (2.11(2) Å) is shortened somewhat relative to the corresponding bonds in the μ-Os−C bonds in the previously reported electron-deficient benzoheterocyclic complexes on becoming terminal.[19] The bridging N(1)−Os(1) and N(1)−Os(3) bonds (2.16(1) and 2.10(3) Å) exhibit a slight asymmetry, and the average is approximately the same in related complexes with terminal N−Os bonds.[19]

Scheme 2

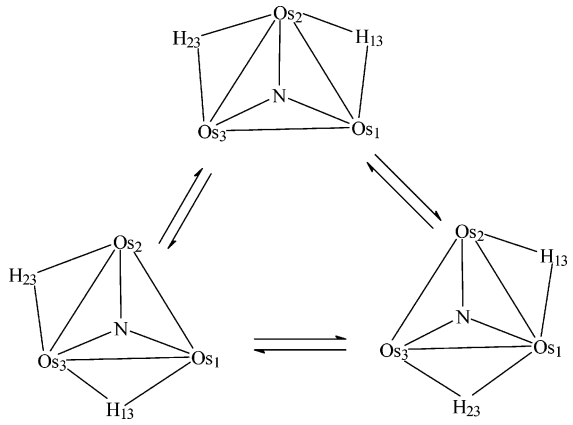

The VT ^{1}H NMR spectra of compound **9** clearly elucidates the nature of the hydride exchange process, on the basis of the solid-state structure (Figure 2). Thus, at −45 °C in $CDCl_3$ we observe two doublet hydride resonances at −14.06 (J = 2 Hz) and −14.10 (J = 2 Hz) ppm and two aliphatic resonances at 5.05 (d, J = 12 Hz) and 3.95 (d, J = 12 Hz) ppm, all of equal relative intensity. As the temperature is increased to room temperature, the hydride resonances average to a single sharp hydride resonance at −14.06 ppm, while the two methylene protons resonances average to a broadened resonance in the range 5.2−3.9 ppm. At −45 °C, 2D-COSY shows these two protons are correlated to each other. The aromatic resonances remained unchanged through the temperature range examined, at 7.21, 6.62, and 6.56 ppm. This behavior is consistent with a process in which one of the hydrides, H(13) (Figure 1), moves from the Os(1)−Os(3) edge to the Os(1)−Os(2) edge to induce a symmetry plane followed by edge-to-edge migration of either hydride (Scheme 2).[6]

This process is directly analogous to that observed for the complexes **5** and **6**. In the case of **6** the symmetrical isomer was detected in very low concentrations.[6] The $\Delta G^{\ddagger}$ value for this process in **9** is estimated to be 13.7 ± 1.4 kcal/mol, which is virtually identical with the 12.7 ± 1.3 kcal/mol estimated for **6**.[6,31]

In sharp contrast to **7**, $Os_3(CO)_9(\mu_3\text{-}\eta^2\text{-}C_7H_3(2\text{-}CH_3)NS)(\mu\text{-}H)$ (**7′**) undergoes nucleophilic attack at the carbocyclic ring on treatment with H^- and after treatment with acid gives the 48e $\sigma-\pi$-vinyl complex $Os_3(CO)_9(\mu_3\text{-}\eta^3\text{-}C_7H_5(2\text{-}CH_3)NS)(\mu\text{-}H)$ (**9′**) in 74% yield using the same reagents and conditions as for **7** (eq 6).

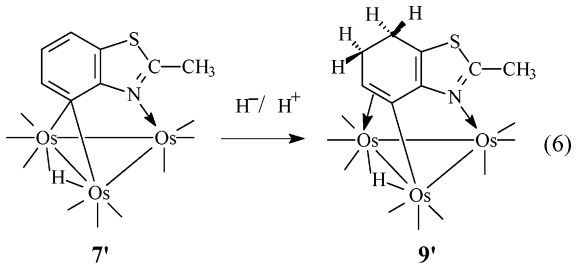

7′ **9′** (6)

This compound was characterized by IR, ^{1}H NMR, and elemental analysis. In the ^{1}H NMR two multiplets of relative intensity 2 appear at 2.65 and 2.38 ppm due to $CH_2(4)$ and CH_2-

(30) Estimated using the formula $\Delta G^{\ddagger} = 4.57T_c(9.97 - \log T_c/\Delta\nu)$, where T_c is the coalescence temperature and $\Delta\nu$ is the difference in chemical shift between two resonances of equal intensity at the low-temperature limit. An error of ±5% in the temperature measurement was assumed.

(31) Abedin, J. Doctoral Thesis, University of Montana, 2002.

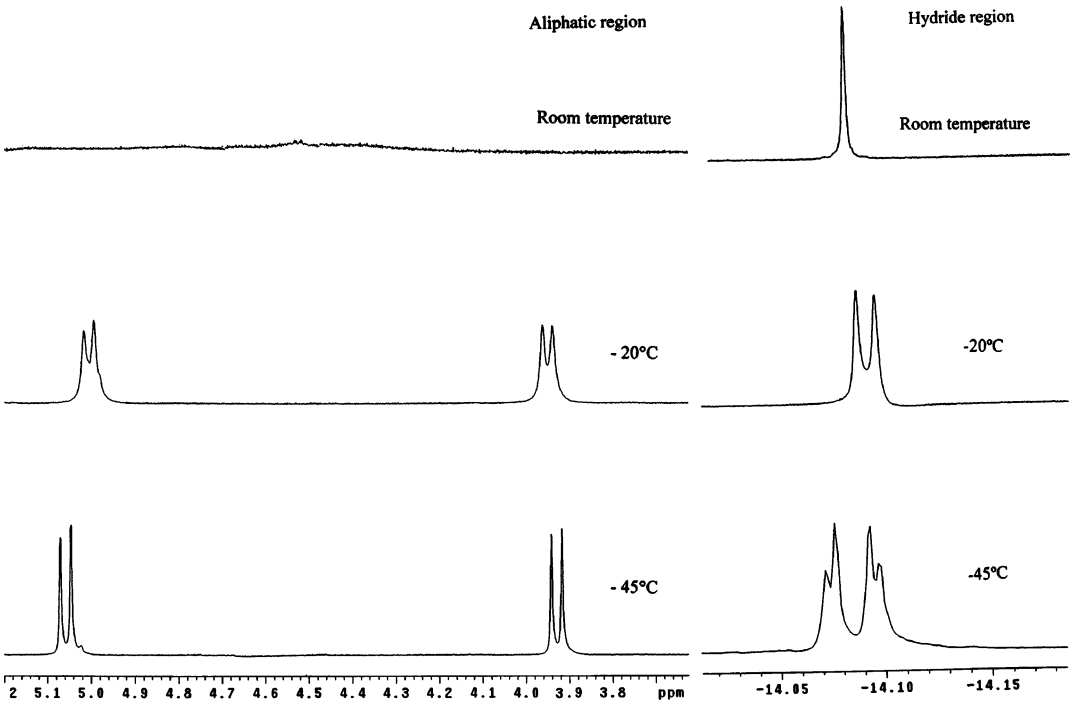

Figure 2. VT ^{1}H NMR of the aliphatic (left) and hydride (right) regions of **9** at 400 MHz in $CDCl_3$.

(5), and the vinyl proton at C-6 is observed as a doublet of doublets at 4.46 ppm. The $-CH_3$ and hydride chemical shifts are obtained as two singlets at 2.62 and −16.93 ppm, respectively. All these data are consistent with the formation of a $\sigma-\pi$-vinyl complex.[4]

The sequential reaction of the benzoxazole complex $Os_3(CO)_9(\mu_3\text{-}\eta^2\text{-}C_7H_4NO)(\mu\text{-}H)$ (**8**) with H^-/H^+ gave $Os_3(CO)_9(\mu_3\text{-}\eta^2\text{-}C_7H_5NO)(\mu\text{-}H)_2$ (**10**) in 41% yield and a trace of a second red product (vide infra) (eq 7). Unlike the case of **7**, when this

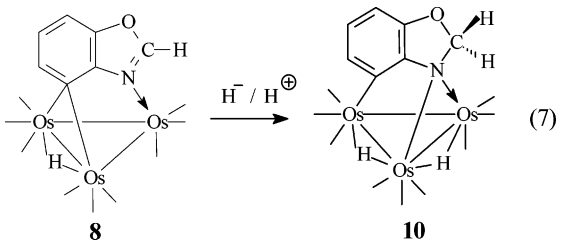

8 **10** (7)

reaction is followed by ^{1}H NMR no evidence of initial protonation at nitrogen is observed. Compound **10** was characterized by ^{1}H NMR and IR spectroscopy and is virtually identical with **9** in every respect, including its VT ^{1}H NMR behavior. Thus, the ^{1}H NMR for **10** at −45 °C shows two sharp hydride resonances at −13.84 and −14.07 ppm and two aliphatic resonances at 5.28 (J = 5 Hz) and 5.04 (J = 5 Hz) ppm. The two aliphatic resonances are coupled to each other in the 2D-COSY at −45 °C. As the temperature is increased, coalescence of these two sets of resonances takes place at about −10 °C, and at room temperature, a single sharp hydride resonance at −13.95 ppm is observed, while the aliphatic resonances average to a slightly broadened resonance at 5.17 ppm. The aromatic resonances remained unchanged throughout this temperature range at 6.96, 6.53, and 6.28 ppm. The $\Delta G^{\ddagger}$ value for this process is estimated to be 11.9 ± 1.2 kcal/mol, which again is very similar to the barriers estimated for **6** and **9**. The 2-methyl-substituted analogue of **8** also undergoes nucleophilic attack at the 2-position, in contrast to the case for **7′**, but this is followed by a ring-opening reaction, leading to a series of interesting compounds whose formation has been mechanistically investigated. The results of these studies are beyond the scope of this paper and will be reported separately.[31]

Kinetics and Equilibrium Constants for the Tautomerization of 9 and 10. When solutions of **9** and **10** are heated in toluene at 90 °C in toluene, they gradually turn from yellow to red and new hydride, aliphatic, and aromatic resonances appear in the ^{1}H NMR spectrum. Chromatographic separation of the heated solution leads to the isolation of the deep red complexes $Os_3(CO)_9(\mu_3\text{-}\eta^2\text{-}(L\text{-}2H))(\mu\text{-}H)_2$ (L = benzothiazole (**11**), benzoxazole (**12**); Scheme 1). These complexes were characterized by ^{1}H NMR and IR spectroscopy. Compound **11** is completely rigid on the NMR time scale up to 90 °C. In the ^{1}H NMR the two hydride resonances are observed at −13.05 (J = 2 Hz) and −13.43 ppm (J = 2 Hz) and the two methylene protons appear as two doublets at 5.02 (J = 12 Hz) and 4.79 ppm (J = 12 Hz). 2D COSY shows that the two methylene protons are coupled to each other. In the aromatic region a doublet of doublets at 6.88 ppm is coupled to a doublet of triplets at 5.34 ppm, which is also coupled to a doublet of doublets at 6.34 ppm. The ^{1}H NMR for **12** at room temperature shows two hydrides as two doublets at − 13.16 (J = 2 Hz) and −13.22 ppm (J = 2 Hz) and two aliphatic resonances at 5.47 (J = 8 Hz) and 5.30 ppm (J = 8 Hz) as doublets as well. The aromatic resonances come at 6.25, 6.14, and 5.50 ppm as two separate doublets and a triplet for C-6, C-4, and C-5 protons, respectively.

Using ^{1}H NMR techniques the tautomeric equilibria, K_{eq}, for **11**/**9** and **12**/**10** were determined to be 1.6 and 3.1, respectively, and the first-order rate constants for the conversion of **9** to **11** and **10** to **12** were determined to be $(6.4 \pm 0.6) \times 10^{-5}$ and $(1.28 \pm 0.1) \times 10^{-4}$ s^{-1} respectively. Here again, the magnitude of these parameters is very similar to those observed for **3** going to **5** and **4** going to **6**, as for observed hydride exchange in **5**, **6**, **9**, and **10**. It is intriguing, however, that for this diverse set of heterocyclic complexes containing both one and two heteroatoms, and both (6,6) and (6,5) ring systems, the relative free energies of the pairs are so similar but the structures of the kinetic products are different and the barriers to their intercon-

Table 3. Calculated (Top) and Experimental (Bottom) Selected Bond Lengths (in Å) for 2, 3, 6, 7, and 9[a]

compd	Os1−C7	Os2−N	Os3−N	N−C9	N1−C2	C4−C5	C5−C6	C6−C7
6	2.14	2.26	2.26	1.47	1.51	1.40	1.40	1.40
	2.14(2)	2.15(1)	2.18(2)	1.46(2)	1.48(2)	1.43(3)	1.40(3)	1.39(3)
7	2.34	2.34	2.24	1.39	1.39	1.39	1.40	1.41
	2.25(1)	2.25(1)	2.14(1)	1.40(2)	1.40(2)	1.41(1)	1.38(1)	1.39(1)
9	2.16	2.18	2.18	1.45	1.49	1.40	1.40	1.40
	2.11(2)	2.10(2)	2.16(2)	1.47(3)	1.51(2)	1.38(5)	1.39(5)	1.38(5)
compd	Os1−C8	Os2−C8	Os3−N	N−C10	N1−C2	C5−C6	C6−C7	C7−C8
2	2.27	2.27	2.21	1.43	1.29	1.40	1.39	1.42
	2.23(2)	2.31(2)	2.14(1)	1.45(1)	1.30(2)	1.33(3)	1.36(2)	1.39(2)
3	2.25	2.24	2.14	1.33	1.47	1.42	1.36	1.46
	2.18(2)	2.18(2)	2.15(1)	1.30(2)	1.44(2)	1.43(3)	1.32(2)	1.47(2)

[a] Experimental values for **3** and **6** are taken from ref 6 and are listed below the calculated values with estimated standard deviations in parentheses. Experimental values for **2** and **7** are taken from refs 6, 19, and 31.

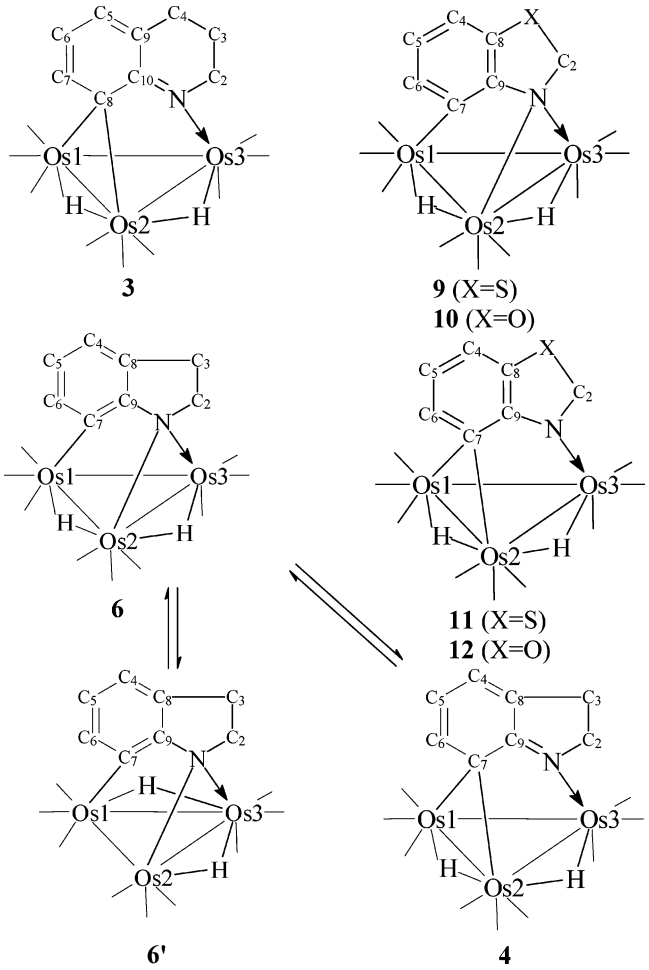

Figure 3. Numbering scheme used for structures used in the tables.

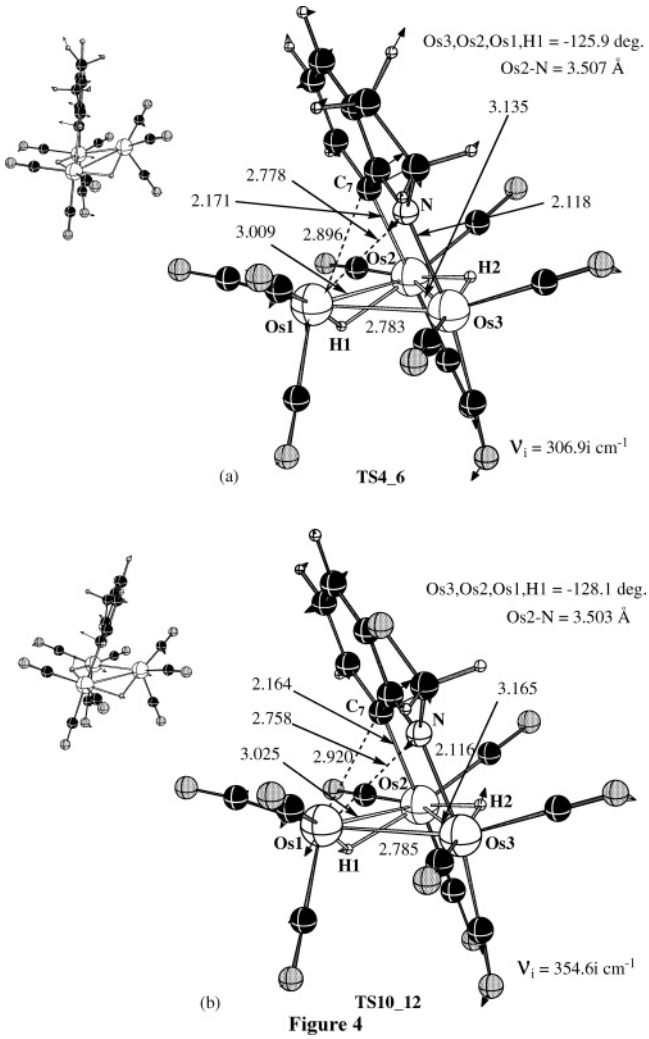

Figure 4. Optimized transition state structures for the interconversion of the tautomeric pairs (a) **4/6** and (b) **10/12**. Bond distances are shown in Å.

version are all so high.[32] For these reasons we have undertaken a detailed computational study of these systems using DFT methods.

Determination of the Transition States and Energy Barriers for the Tautomeric Equilibration of 3/5, 4/6, 9/11, and 10/12 and for the Hydride Migrations in 5, 6, 9, and 10. The tautomeric pairs presented above represent an unusual class of heterocycle-containing molecules in that their equilibrium constants are relatively small, yet their rates of interconversion are relatively slow. The more common situation is one where heterocyclic tautomers of similar energy undergo rapid exchange.[33] This is undoubtedly due to the fact that, in the cases under consideration here, the bonding mode to the cluster is changed in a manner that involves the formal cleavage of metal−carbon or metal−nitrogen bonds as well as rearrangement of the bonding pattern within the ring. Given the similarity of the electronegativities of zerovalent osmium and carbon, one would expect that the transition states for these tautomerizations would be relatively nonpolar and would involve a concerted

(32) Zelenin, K. N.; Aleseyev, V. V. *Top. Heterocycl. Syst.: Synth., React. Prop.* **1996**, *1*, 141.

(33) See for example: Rybtchinski, B.; Oevers, S.; Montag, M.; Vigalok, A.; Rozenberg, H.; Martin, J. M. L.; Milstein, D. *J. Am. Chem. Soc.* **2001**, *123*, 9064.

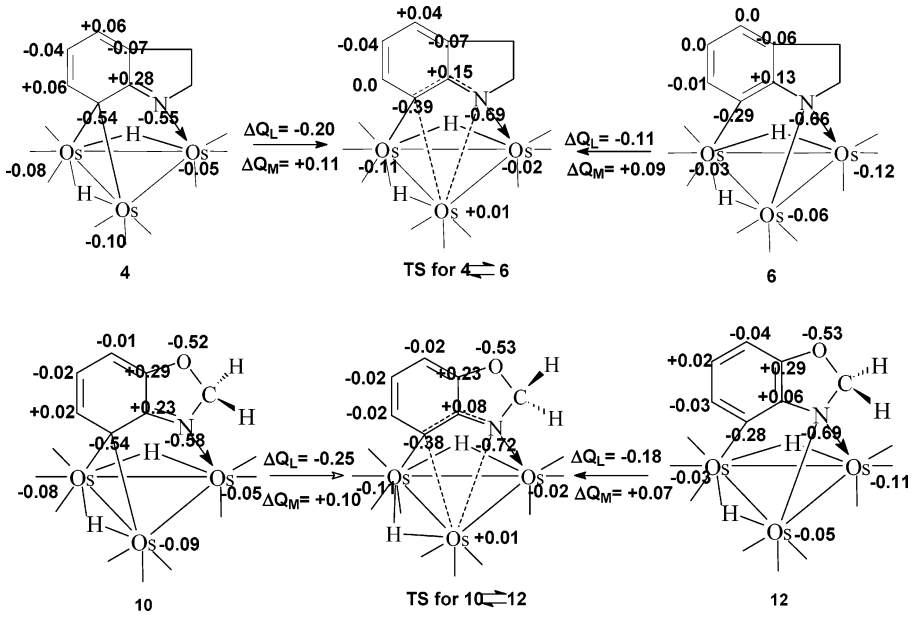

Figure 5. Natural population analysis net charges on atoms (summed over the atoms for CH and CH_2) in the transition states and the minima involved in the tautomerizations of **4** to **6** and **10** to **12**.

Table 4. Experimental ΔG° and $\Delta G^\ddagger$ Values and Calculated ΔG°, ΔH° and $\Delta G^\ddagger$, $\Delta H^\ddagger$ Values (in kcal/mol) for the Tautomeric Equilibria 5/3, 6/4, 11/9, and 12/10

tautomeric pair	ΔG°(exptl)	ΔG°(calcd)	ΔH°(calcd)	$\Delta G^\ddagger$(exptl)	$\Delta G^\ddagger$(calcd)	$\Delta H^\ddagger$(calcd)	imag freq (cm^{-1})
5/3	-1.07 ± 0.1	+1.36	+0.36	29.0 ± 3			
6/4	-1.07 ± 0.1	+0.11	−0.93	28.3 ± 3	31.5	31.2	307i
11/9	-0.44 ± 0.1	−1.15	−0.05	28.3 ± 3			
12/10	-1.00 ± 0.1	−1.09	−0.04	27.8 ± 3	31.6	30.7	354i

multicenter configuration. To test this hypothesis, we have performed B3LYP calculations on the structural pairs **3/5**, **4/6**, **9/11**, and **10/12** and a search for transition states for the interconversion of the **4/6** and **10/12** pairs.

A comparison of the experimental and calculated selected bond lengths for **2**, **3**, **6**, **7**, and **9**, for which solid-state structures have been obtained, is shown in Table 3 using the numbering system shown in Figure 3. From this table it can be seen that there is good agreement between the calculated and experimental bond lengths for the intraligand bonds and for the terminal nitrogen−osmium and carbon−osmium bonds (the Os−Os bonds were also in good agreement, not shown in the table). However, the calculated values for the bridging carbon−osmium (in **2**, **3**, and **7**) and the bridging nitrogen−osmium (in **6** and **9**) bonds are slightly elongated with respect to the experimental values. This could be due to lack of an f-polarization function for the metal atoms in our calculations.[34] More importantly, the key features that differentiate the two tautomeric structures are reproduced by the calculations: i.e., the disruption of the aromaticity in the carbocyclic ring on going from structural types **6** and **9** to structural type **3**, where we see formation of a C−N double bond and the introduction of alternating short and long C−C bonds in the carbocyclic ring.

Except for the tautomeric pair **5/3**, the calculated ΔG° values, and hence the equilibrium constants, are in reasonable agreement with the experimental values (Table 4). In the case of the **5/3** equilibrium, the relative stabilities of the two tautomers are inverted, but considering the expected accuracy of the DFT calculations (±2−3 kcal/mol),[35] the calculated relative free energies and enthalpies are reasonable. The important point is that the calculations show that the tautomeric pairs are of very similar energies.

Since the experimental standard free energies and free energies of activation are so similar for the series, we chose to study two of the four pairs, **4** to **6** and **10** to **12**. The former has fewer atoms and gave a standard free energy difference for the tautomeric pair in better agreement with the experimental value, and the latter has only first-row elements in the ligand, which are best suited for the basis sets chosen. As mentioned above, the bonding interactions between the heterocycle and the low-valent osmium core are likely to be fairly nonpolar in nature. Given this, a transition state for the conversion of **4** to **6** is expected to involve the simultaneous elongation of the C7−Os2 and N−C9 distances and shortening of the N−Os2 and C7−C9 distances (Figure 3).

Exactly the same transition state is expected for the rearrangement of **10** to **12**, but elongation of the N−Os2 and C7−C9 bonds and shortening of the C7−Os2 and N−C8 distance are required. A computational search indeed led to the expected transition states shown in parts a and b of Figure 4. The activation parameters and imaginary frequencies corresponding to the reaction coordinate of these transition states are shown in Table 4.

The agreement of the calculated free energies of the transition states (relative to the reactants) with the experimental free energies of activation from the kinetic data is quite reasonable, with errors of 3−4 kcal/mol expected for B3LYP calculations. As seen in Figure 4, at **TS4_6**, for instance, the C_7-Os_1 bond to be broken is stretched to 2.87 Å from 2.32 Å in the reactant **4** and the $N-Os_2$ bond to be formed is longer at 2.78 Å compared to 2.20 Å in the product **6**. The transition state is "synchronous", as the C_7-Os_2 bond breakage and the $N-Os_2$ bond formation are taking place rather simultaneously. The

(34) Lynch, B. J.; Fast, P. L.; Harris, M.; Truhlar, D. G. *J. Phys. Chem. A* **2000**, *104*, 4811.

(35) Musaev, D. G.; Hirao, K. *J. Phys. Chem. A* **2003**, *107*, 1563.

vibrational mode associated with the reaction coordinate involves major motions of the nitrogen, ring C, CH, and CH_2 groups as well as a slight motion of the hydride ligand. The significance of these results is that the relatively high barriers observed for these tautomerizations are associated with concerted reorganization of the bonds within the ligand and in the metal−ligand bonds rather than with bond readjustments in the metal core or with hydride migrations (which should have a low barrier), as has been proposed for cluster processes involving carbonyl ligands and or acyclic hydrocarbons.[37]

Further insight into the nature of the transition state is gained by a natural population analysis[24] of the tautomers and the associated transition states. Figure 5shows the charges on the atoms involved in the transition state and the net charge on the CH groups conjugated with them. In comparison to the tautomers **4** and **6** or **10** and **12**, there is a significant decrease in negative charge at the metal core in the corresponding transition states (**4** to **TS**, $\Delta Q_M = +0.11$e; **6** to **TS**, $\Delta Q_M = +0.09$e; **10** to **TS**, $\Delta Q_M = +010$ e; **12** to **TS**, $\Delta Q_M = +0.07$e). The net charges on the CH_2 groups remain constant within each series, but there is a significant increase in the overall negative charge on the ligand on summation of the net charges of the other atoms in the ligand (Figure 5). Thus, for **4** to **TS** $\Delta Q_L = -0.20$e, for **6** to **TS** $\Delta Q_L = -0.11$e, for **10** to **TS** $\Delta Q_L = -0.25$e, and for **12** to **TS** $\Delta Q_L = -0.18$e. Although the transition state can be thought of as essentially nonpolar, there is significant charge separation in the transition state relative to either tautomeric form. Furthermore, this analysis reveals that the μ-alkylidene−imino tautomer donates more electron density to the metal core than the μ-amido−aryl tautomer, because there is less negative charge on the ligand in the former. That the charge on the metal core is the same for both tautomers suggests that the carbonyl ligands accept more electron density in the μ-alkylidene−imino tautomer, especially since the charge on hydrides is constant in the tautomeric pairs.[38]

The conclusion that the hydride ligands do not play a major role in the tautomerization is underscored by the fact that the pseudo-IRC calculation going from the transition state to **6** gives the symmetrical hydride isomer of **6′** (Figure 3), which lies only 1.65 kcal/mol above **6** in free energy. Here we investigated the barrier to hydride migration in this class of molecules, for which the experimentally reported value of the barrier is 12.7 kcal/mol in the case of **6**.[6] We have explored two possible pathways: (1) via the formation of terminal hydride species, which has been shown to be operative in previous computational studies involving metal to ligand hydrogen transfers and has been invoked as the most probable intermediate for hydride migrations in clusters,[11,36] and (2) via the formation of face-bridging hydride either symmetrically or asymmetrically bound to the cluster face, which has been observed in many isolable complexes.[37] Calculations show that the terminal hydride pathway has a barrier of 16.1 kcal/mol (see Figure 6a). This optimized transition state has an imaginary frequency of 103i cm^{-1} that corresponds to the reaction coordinate involving a terminal Os−H (1.66 Å). The performed pseudo-IRC calculations along this vibrational mode confirmed that this is a transition state connecting **6** to **6′**. Meanwhile, the asymmetrical face-bridging pathway occurs via a transition state with H−Os1, H−Os2, and H−Os3 distances of 2.21, 1.76, and 1.82 Å (Figure 6b), respectively. It has an imaginary frequency of 429i cm^{-1}

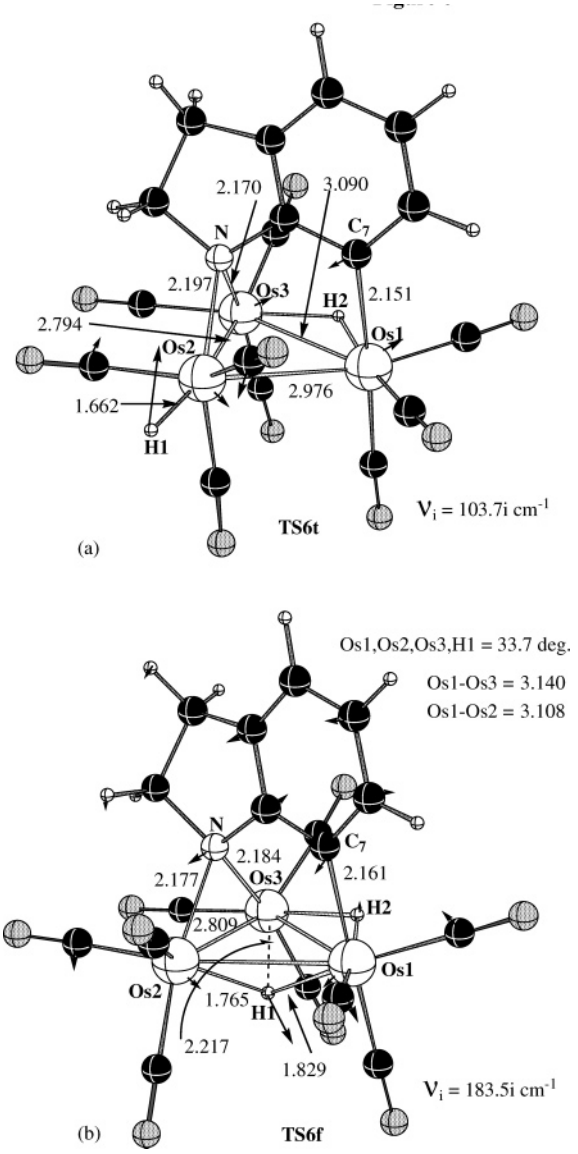

Figure 6. Optimized structures of (a) the terminal hydride transition state and (b) the asymmetrically face-bridged transition state for hydride migration from **6**. Bond distances are shown in Å.

and was confirmed (by performing pseudo-IRC calculations) to also connect **6** with **6′**. The calculated free energy of activation at this transition state is 12.3 kcal/mol relative to **6′**. Thus, the calculated difference in the barriers between these two pathways is 3.7 kcal/mol, corresponding to a factor of 1500 in the rate constant for hydrogen migration, thus favoring the asymmetrically bridged intermediate. Although the absolute errors in barrier height are ca. 3−5 kcal/mol, the relative error between similar reactions is expected to be much smaller and the conclusion should be qualitatively correct. To our knowledge, this represents the first definitive evidence that points to the lower energy of the face-bridged hydride relative to a terminal hydride as the transition state for hydrogen migration in trimetallic transition-metal carbonyl clusters. Previous Fenske−Hall and extended Hückel molecular orbital calculations and experimental studies have pointed to the feasibility of η^3-hydrides as transition states for hydride migrations in tetranuclear transition-metal carbonyl clusters.[38,39] The calculations show that the symmetrically face-bridged hydride structure (where all three Os−H distances are equal) lies less than 1 kcal/

(36) Rosenberg, E. *Polyhedron* **1989**, *26*, 1.
(37) For a recent example see: Cabeza, J. A.; Del Rio, I.; Garcia-Alvarez, P.; Miguel, D.; Riera, V. *Inorg. Chem.* **2004**, *43*, 5450.
(38) Howells, A. R.; Milletti, C. *Inorg. Chim. Acta* **1993**, *203*, 43.
(39) Farrugia, L. J. *Organometallics* **1989**, *8*, 2410.

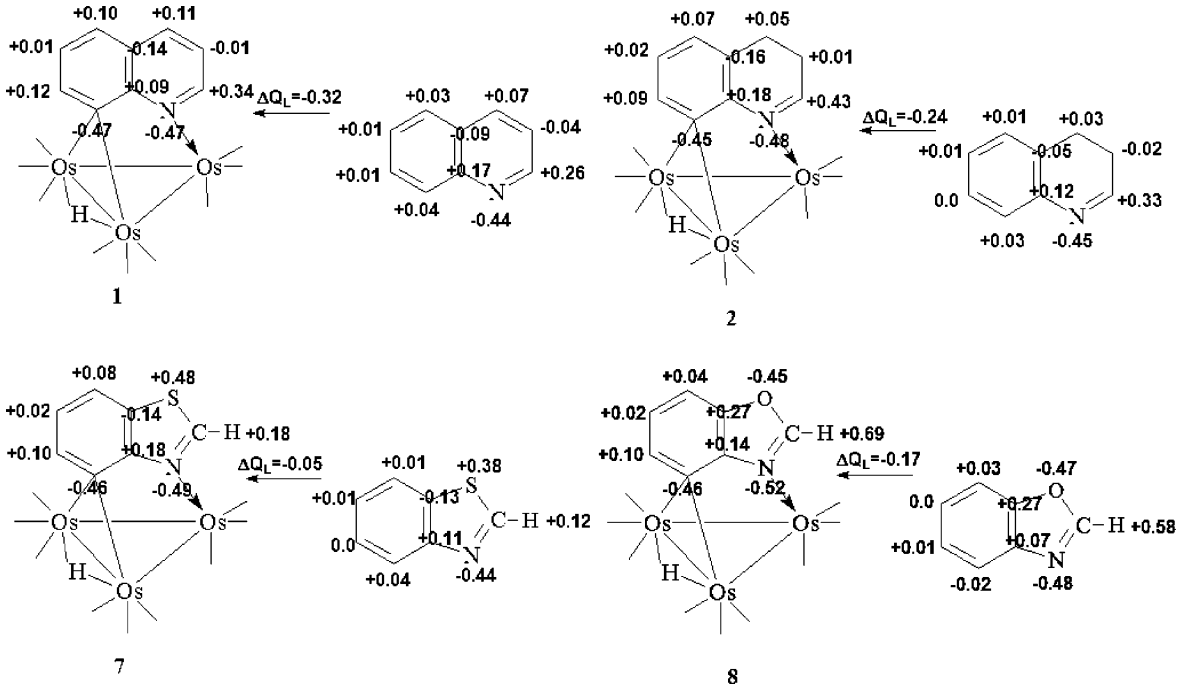

Figure 7. Natural population analysis net charges on atoms (summed over the atoms for CH and CH_2) for complexes **1**, **2**, **7**, and **8** and their corresponding free ligands.

mol above the calculated asymmetric transition state and is not an important point on the potential energy surface in the conversion of **6** to **6′**.

Natural Population Analysis for Evaluating the Site of Nucleophilic Attack. We previously reported that the reason the site of nucleophilic attack in complexes such as **1** was changed from the 5-position (in **1**) to the 2-position (in **2**) upon adding H^- and H^+ was related to the disposition of the LUMO in the complex relative to the free ligand.[40] This approach gave good agreement with experiment for several systems and explained both the chemical and spectroscopic properties of a range of heterocyclic complexes.[40,41] However, in molecules as complex as those discussed here, where there are many similar LUMO's, it can be dangerous to assign chemistry on the basis of the properties of one of many virtual orbitals. We therefore undertook a natural population analysis[24] of complexes **1**, **2**, **7**, **8**, and related intermediates, as shown in Figure 7, to see if charge distributions could explain the observed reactivities of these complexes and would support some of the conclusions stated above. The charge distributions of a free ligand and the metal core should be directly related to the electrostatic interaction, and that of the complex relative to the components reflects the extent of the intraligand polarization and the ligand−metal charge transfer.

The NPA reveals that there is no net electron density withdrawal from the heterocyclic ring. Indeed, there is a slight increase in net electron density relative to the free ligand (ΔQ = −0.32 for **1**, −0.24 for **2**, −0.05 for **7**, and −0.17 for **8**; Figure 7). However, there is a strong polarization of charge within the ligand, which is most apparent at the carbon atom bridging the two osmium atoms. Thus, the so-called electron-deficient bonding mode (the total valence electron count for the cluster is 46e while the effective atomic number rule requires 48e) is more appropriately viewed in terms of strong polarization of electron density within the heterocycle. Interestingly, the net charge on the metal atoms is −0.26e and is −0.14 to −0.16e on the hydride, with the carbonyl groups bearing a net positive charge. The details of these trends are discussed elsewhere.[42]

In the particular case of quinoline the positions in the ring with the most positive net charge correspond qualitatively to the places where nucleophilic attack has been observed. Thus, nucleophilic attack at the 7-position and the 4-position has been observed when the 5-position is blocked.[4,43] However, the differences in positive charge are small and cannot explain the fact that even with the relatively small nucleophile H^- nucleophilic attack takes place exclusively at the 5-position.[4,5] In considering the factors controlling the site of nucleophilic attack, one must consider the stability of the resulting anion as well as the charge distribution in the reactant. Indeed, DFT calculations on the four possible anions reveals that the anion resulting from nucleophilic attack at the 5-position is 6−8 kcal/mol more stable than the other three (Figure 8). This is likely due to more efficient delocalization of charge to the metal core and the carbonyl ligands, but this is not particularly evident from the NPA calculations, where only slight differences in the charge on the metal core are observed. In the case of the 3,4-dihydroquinoline ligand complex **2**, nucleophilic attack at the 5-position leads to an anion that is ∼18 kcal/mol higher in energy than attack at the 2-position. It would appear that in this case loss of conjugation in the carbocyclic ring outweighs the larger degree of polarization within the ligand suggested by the NPA calculations. Attack at the 2-position is also clearly favored by the very large difference in positive charge at this location relative to the other positions in the ring (Figure 7).

The cases of the benzothiazole and benzoxazole complexes **7** and **8** are quite clear-cut, where the net positive charge at the 2-position is far greater than the charges at the other positions in the ring (Figure 7). Apparently, substitution of an electron-

(40) Nervi, C.; Gobetto, G.; Milone, L.; Viale, A.; Rokhsana, D.; Fiedler, J. Rosenberg, E. *Chem. Eur. J.* **2003**, *9*, 5749.

(41) Rosenberg, E.; Rokshsana, D.; Nervi, C.; Gobetto, R.; Milone, L.; Viale, A.; Fiedler, J. *Organometallics* **2004**, *23*, 215.

(42) Nowroozi, T.; Musaev, D. G.; Morokuma, K.; Rosenberg, E. *Organometallics* **2005**, *24*, 5973.

(43) Rosenberg, E.; Smith, R.; Hardcastle, K. I.; Vasquez, V.; Roh, J. *Organometallics* **1999**, *18*, 3519.

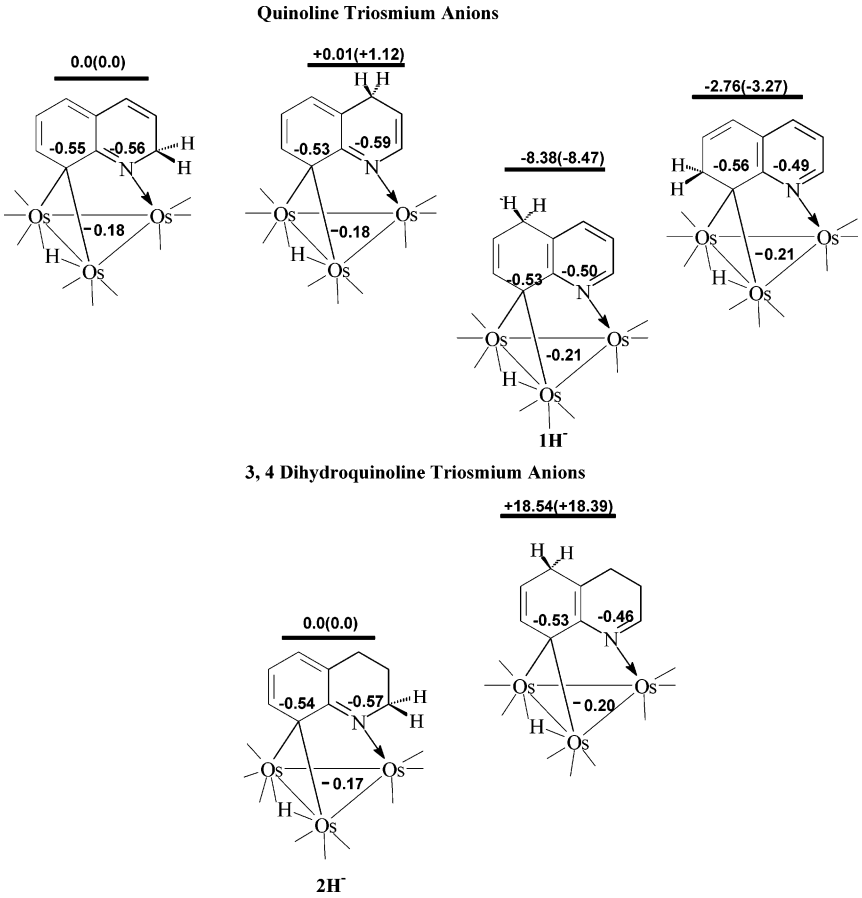

Figure 8. Relative enthalpies (free energies in parentheses, in kcal/mol) for various anions generated by hydride addition to **1** and **2**.

donating methyl group for hydrogen in the case of **7** is sufficient to switch the site of attack to the 4-position, where the difference in net positive charge is 0.10e, whereas in the case of **8** the difference is 0.65e and methyl substitution is not sufficient to change the site of nucleophilic attack by hydride.

Conclusions

The DFT calculations using the well-established B3LYP functional and standard basis sets give optimized structures and stationary point energies that are in reasonable agreement with solid-state structural data and with the relative energies of the tautomeric pairs **5/3**, **6/4**, **11/9**, and **12/10**. The transition states developed give barriers that are in reasonable agreement with experimental estimates from single-point rate constant estimates. More importantly, the transition states determined provide a good qualitative picture of how the tautomerizations occur. They involve some redistribution of charge relative to the reactant minima but are essentially nonpolar in nature. The four-center transition states involve significant reorganization of the bonds between the metal and the ligand and within the heterocycle but not the metal−metal or metal−hydride bonds. Subsequent calculations on the structures obtained from pseudo-IRC calculations on the transition states revealed that an unsymmetrical face-bridging hydride is a more favorable transition state for hydride exchange than a terminal hydride in these dihydride structures.

Finally, the DFT calculations have shown that the sites of nucleophilic attack in the complexes **1**, **2**, **7**, and **8** are determined by the changes in charge distribution in the complexes relative to the free ligand and in some cases by the relative stability of the resulting anions or a combination of these two factors.

Acknowledgment. Support for this research by the Department of Energy (E.R., Grant No. DE-FG02-01ER45869) and National Science Foundation (K.M. and D.G.M., Grant No. CHE-0209660) is gratefully acknowledged. E.R. wishes to thank the Cherry Emerson Center for Scientific Computation for a Visiting Fellowship Award and for use of its computational resources.

Supporting Information Available: Text giving the complete ref 24, tables giving Cartesian coordinates (in Å) for all structures reported in this paper (Table 1S), and a CIF file for structure **9**. This material is available free of charge via the Internet at http://pubs.acs.org.

OM050719L